

Report Title

Controlling solid state nuclear spins

ABSTRACT

The goal of this project was to improve our control over nuclear spins in the solid state, and to extend this control to coupled electron-nuclear spins. Our key results are summarized below.

1. We extended the control techniques developed in liquid state NMR quantum information processing to the control of a three-qubit solid state NMR quantum information processor.
 2. To explore multi-body spin dynamics and their sensitivity to decoherence, we have measured the decay of NMR multiple quantum coherence intensities in the presence and absence of the dipolar Hamiltonian, in a cubic and a one-dimensional spin system.
 3. We also studied the transport of polarization in the one-dimensional fluoroapatite system, both experimentally and theoretically, and created special states in which the polarization is localized to the ends of the chain. This enables both universal Quantum Computing and Quantum Simulation in 1-D systems.
 4. We devised a novel scheme for electron-nuclear quantum information processing that exploits the anisotropic hyperfine coupling. This scheme enables universal control over a 1-electron, N-nuclear spin system, addressing only a single electron spin transition. Not having to address the nuclear spins directly significantly speeds up the control. We designed and fabricated a pulsed electron spin resonance spectrometer, along with a cryogenic probe which we used to experimentally implement this scheme on a single crystal sample of irradiated malonic acid.
 5. We demonstrated the role of nuclear spin dipolar diffusion in dynamic nuclear polarization (DNP) experiments, in dielectric samples with abundant nuclear spins. We achieved a ^{29}Si polarization of 8.3% at 66 GHz and 1.1 K in single crystal P-doped, the highest ever reported, using DNP.
-

List of papers submitted or published that acknowledge ARO support during this reporting period. List the papers, including journal references, in the following categories:

(a) Papers published in peer-reviewed journals (N/A for none)

1. "NMR Quantum Information Processing", C. Ramanathan, N. Boulant, Z. Chen, D. G. Cory, I. Chuang and M. Steffen, *Quantum Information Processing*, 3, 15-44 (2004).
2. "Entanglement Assisted Metrology", P. Cappellaro, J. E. Emerson, N. Boulant, C. Ramanathan, S. L. Lloyd and D. G. Cory, *Physical Review Letters*, 94, Article 020502 (2005).
3. "On the hydrodynamic approach to coherent nuclear spin transport in solids", D. Greenbaum, M. Kindermann, C. Ramanathan and D. G. Cory, *Physical Review B*, 71, Article 054403 (2005).
4. "Selective coherence transfers in homonuclear dipole coupled spin systems", C. Ramanathan, S. Sinha, J. Baugh, T. F. Havel and D. G. Cory, *Physical Review A*, 71, Article 020303 (2005).
5. "Multi-spin dynamics of the NMR free induction decay", H. Cho, T. D. Ladd, J. Baugh, D. G. Cory and C. Ramanathan, *Physical Review B*, 72, Article 054427 (2005).
6. "Solid state NMR three-qubit homonuclear system for quantum-information processing: Control and characterization", J. D. Baugh, O. Moussa, C. A. Ryan, R. Laflamme, C. Ramanathan, T. F. Havel, D. G. Cory, *Physical Review A*, 73, 022305 (2006).
7. "Decay of highly correlated spin states in a dipolar-coupled solid: NMR study of CaF_2 ", H. Cho, P. Cappellaro, D. G. Cory and C. Ramanathan, *Physical Review B*, 74, 224434 (2006).
8. "Single spin measurement using cellular automata techniques", *Physical Review Letters*, 97, Article 100501 (2006).
9. "A nuclear spin valve: Towards the read-out of single nuclear spin qubits", M. Kindermann, D. G. Cory, *Quantum Information Processing*, 6, 127-136 (2007).
10. "Low temperature probe for dynamic nuclear polarization and multiple-pulse solid-state NMR", H. Cho, J. D. Baugh, C. A. Ryan, D. G. Cory and C. Ramanathan, *Journal of Magnetic Resonance*, in press. (2007)

Number of Papers published in peer-reviewed journals: 10.00

(b) Papers published in non-peer-reviewed journals or in conference proceedings (N/A for none)

Number of Papers published in non peer-reviewed journals: 0.00

(c) Presentations

1. Entanglement Assisted Metrology, D. G. Cory, NMR Sensors Conference, Washington DC (2004).
2. Tutorial on the use of nuclear spins for QIP, D. G. Cory, APS March Meeting, Montreal, Canada (2004).
3. NMR Approaches to QIP, D. G. Cory, Physics Simulations by Quantum Computing Conference, Martha's Vineyard MA (2004).
4. Quantum Metrology, D. G. Cory, Spin Technology Conference, San Francisco CA (2004).
5. Spin gyroscopes and Metrology, D. G. Cory, Quantum Information Science and Technology, San Francisco CA (2004).
6. NMR Approaches to QIP, D. G. Cory, Optical Society of America (2006).
7. Principles and Applications of Control in Quantum Systems, D. G. Cory, Harvard University (2006).
8. NMR Approaches to QIP, D. G. Cory, Japan/US workshop on Quantum Computing (2006).
9. Universal Control of nuclear spins via anisotropic hyperfine interactions, J. Hodges, PRACQSYS, Cambridge MA (2006).
10. Hyperfine couplings in silicon, C. Ramanathan, Aspen Condensed Matter Conference Aspen CO (2007).
11. Universal control via anisotropic hyperfine couplings, C. Ramanathan, International Conference on Nanoelectronics, Nanostructures and Carrier Interaction(NNCI), Atsugi, Japan (2007).

Number of Presentations: 11.00

Non Peer-Reviewed Conference Proceeding publications (other than abstracts):

Number of Non Peer-Reviewed Conference Proceeding publications (other than abstracts): 0

Peer-Reviewed Conference Proceeding publications (other than abstracts):

Number of Peer-Reviewed Conference Proceeding publications (other than abstracts): 0

(d) Manuscripts

1. "Rapid Diffusion of dipolar order enhances Dynamic Nuclear Polarization", A. E. Dementyev, D. G. Cory, C. Ramanathan.
2. "Dynamic Nuclear Polarization in Silicon Nanoparticles", A. E. Dementyev, D. G. Cory, C. Ramanathan.
3. "Dynamics and control of a quasi-1D spin system", P. Cappellaro, C. Ramanathan, D. G. Cory.
4. "Simulations of Information Transport in Spin Chains", P. Cappellaro, D. G. Cory.
5. "Universal Control of a coupled electron-nuclear spin system via the anisotropic hyperfine interaction", J. S. Hodges, J. C. Yang, C. Ramanathan, D. G. Cory.
6. "Encoding nuclear spin logical qubits in a coupled electron-nuclear spin system", J. Hodges, C. A. Ryan, C. Ramanathan, D. G. Cory.

Number of Manuscripts: 6.00

Number of Inventions:

Graduate Students

<u>NAME</u>	<u>PERCENT SUPPORTED</u>
Jonathan Hodges	0.83
FTE Equivalent:	0.83
Total Number:	1

Names of Post Doctorates

<u>NAME</u>	<u>PERCENT SUPPORTED</u>
FTE Equivalent:	
Total Number:	

Names of Faculty Supported

<u>NAME</u>	<u>PERCENT SUPPORTED</u>	National Academy Member
David Cory	0.00	No
FTE Equivalent:	0.00	
Total Number:	1	

Names of Under Graduate students supported

<u>NAME</u>	<u>PERCENT SUPPORTED</u>
FTE Equivalent:	
Total Number:	

Student Metrics

This section only applies to graduating undergraduates supported by this agreement in this reporting period

The number of undergraduates funded by this agreement who graduated during this period:

The number of undergraduates funded by this agreement who graduated during this period with a degree in science, mathematics, engineering, or technology fields:.....

The number of undergraduates funded by your agreement who graduated during this period and will continue to pursue a graduate or Ph.D. degree in science, mathematics, engineering, or technology fields:.....

Number of graduating undergraduates who achieved a 3.5 GPA to 4.0 (4.0 max scale):.....

Number of graduating undergraduates funded by a DoD funded Center of Excellence grant for Education, Research and Engineering:.....

The number of undergraduates funded by your agreement who graduated during this period and intend to work for the Department of Defense

The number of undergraduates funded by your agreement who graduated during this period and will receive scholarships or fellowships for further studies in science, mathematics, engineering or technology fields:

Names of Personnel receiving masters degrees

NAME

Total Number:

Names of personnel receiving PHDs

NAME

HyungJoon Cho

Paola Cappellaro

Suddhasattwa Sinha

Total Number:

3

Names of other research staff

NAME

Chandrasekhar Ramanathan

PERCENT SUPPORTED

0.27 No

FTE Equivalent:

0.27

Total Number:

1

Sub Contractors (DD882)

Inventions (DD882)

Scientific Progress (45013PHQC)

The goal of this project was to improve our control over nuclear spins in the solid state, and to extend this control to coupled electron-nuclear spins. Our key results are summarized below.

1. We have measured the decay of NMR multiple quantum coherence intensities both under the internal dipolar Hamiltonian as well as when this interaction is effectively averaged to zero, in the cubic calcium fluoride (CaF₂) spin system and the pseudo one-dimensional system of fluoroapatite.
2. We also studied the transport of polarization in the one-dimensional fluoroapatite system, both experimentally and theoretically, and created special states in which the polarization is localized to the ends of the chain.
3. We extended the control techniques developed in liquid state NMR quantum information processing to the control of a three-qubit solid state NMR quantum information processor.
4. We devised a novel scheme for electron-nuclear quantum information processing that exploits the anisotropic hyperfine coupling. This scheme enables universal control over a 1-electron, N-nuclear spin system, addressing only a single electron spin transition. Not having to address the nuclear spins directly significantly speeds up the control. We designed and fabricated a pulsed electron spin resonance spectrometer, along with a cryogenic probe which we used to experimentally implement this scheme on a single crystal sample of irradiated malonic acid.
5. We demonstrated the role of nuclear spin dipolar diffusion in dynamic nuclear polarization (DNP) experiments, in dielectric samples with abundant nuclear spins. We achieved a ²⁹Si polarization of 8.3% at 66 GHz and 1.1 K in single-crystal P-doped, the highest ever reported, using DNP.

Multiple quantum dynamics in extended spin networks

In solids it is possible to create states that show long-range correlations among the crystal spins, with a high degree of entanglement. The dynamics of these states have been studied in the spectroscopy literature for many years, but an exact understanding of the dynamics is precluded by its complexity. On the other end, an analytical solution for 1D models is possible using the fermionic operators, taking into account nearest-neighbor couplings only. The possibility to experiment on a quasi-1D system is therefore of particular interest to study the crossover from a pure 1D dynamics, which can be simulated classically in an efficient way, to a 3D dynamics, where an exact classical simulation is prohibited by the size of the Hilbert space of interest.

The systems we use are calcium fluoride (CaF₂) and fluoroapatite (FAP). The fluorine spins in CaF₂ form a cubic lattice, while FAP presents linear chains of spins. Figure 1 shows the growth of multi-spin correlations that are developed during the free induction decay following a $\pi/2$ pulse applied to the spin system. The growth of quantum coherences shows an initial oscillation between the zero and double coherence operators (which can be reproduced by a 2-spin model of the evolution) followed at later times by a sigmoidal growth of the higher coherence orders. In the case of a linear spin chain, the

oscillations (predicted by the fermionic solution) last longer, until next-nearest neighbors and later inter-chain interactions come into the play. As a consequence, the growth rate of higher coherences is much slower.

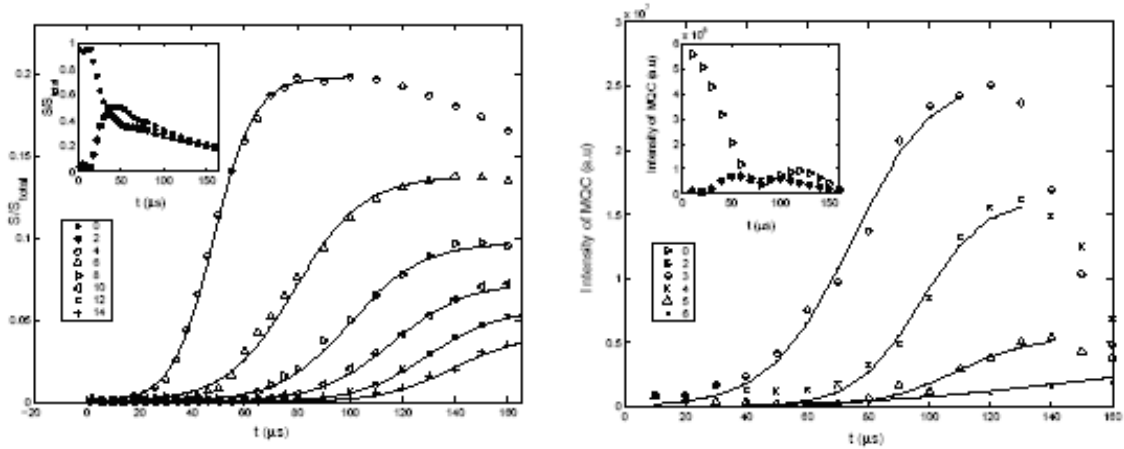


Figure 1. Growth of multiple spin correlations (normalized to the total signal for that evolution time to compensate for imperfect refocusing) showing sigmoidal fit to the initial growth of each coherence order. The insets show the dynamics of 0 and 2 coherence orders. Left: CaF₂ along the [110] direction, Right: Fluorapatite.

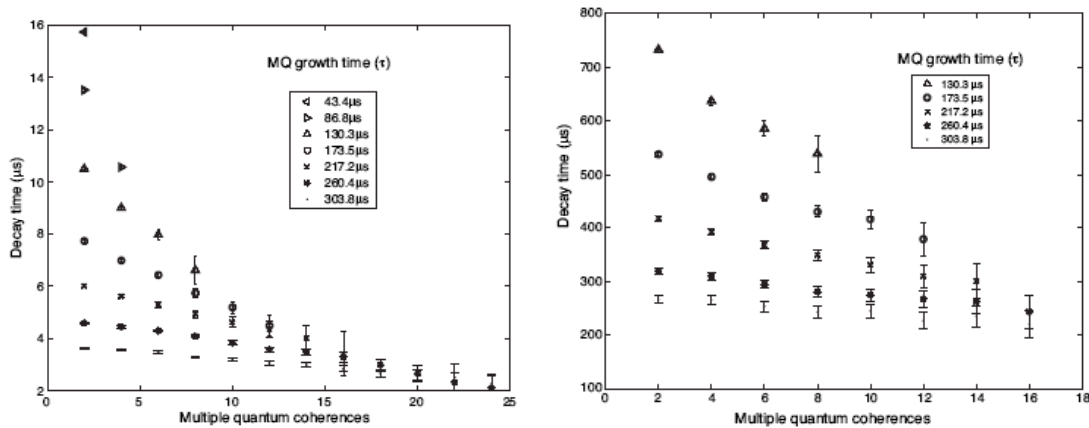


Figure 2. Decay of multiple quantum coherences in CaF₂ during evolution under the internal dipolar Hamiltonian and during an NMR pulse sequences that averages the dipolar coupling to zero.

We also examined the decay of multiple quantum coherences, both under the action of the internal dipolar Hamiltonian of the spin system, as well as under our best efforts to control this evolution. The signals were observed to decay in time as a Gaussian function. We used the standard deviation of the gaussian as the characteristic decay time T_d . Figure 2 shows the decay times of multiple quantum coherences under the dipolar Hamiltonian (left), and under a pulse sequence designed to suspend dipolar evolution (right). It is seen that the scaling behaviour is identical in the two cases. We fit the

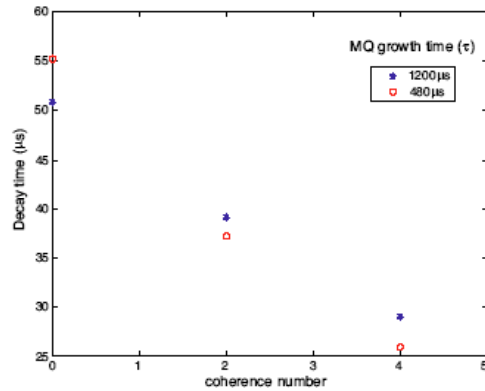
measured decay times and obtained the following general scaling behaviour for the cubic calcium fluoride system.

$$T_d = \frac{A}{\sqrt{N}} - \frac{B \cdot n}{N}$$

where N is the number of correlated spins and n is the coherence order.

A similar, albeit slower dynamics is also observed in the one-dimensional fluoroapatite system as seen in Figure 3. The coherence decay in the one dimensional fluoroapatite system did not change significantly as a function of the multiple quantum growth time, in contrast to the calcium fluoride case. While the growth of coherence orders is severely restricted in this case, the number of correlated spins should continue to grow.

Figure 3.



Transport in one dimensional spin-chains

We then proceeded to investigate the dynamics of the one-dimensional spin system in greater detail. One dimensional spin chains have been proposed as a bus to transfer information from one part of a quantum computer to another. The dynamics of a one dimensional spin chain with only nearest neighbor couplings of the form of an Ising, XY or double quantum Hamiltonian are exactly solvable. However, the spins in a real spin chain are coupled together via dipolar interactions, and no solution exists for this interaction.

An infinite linear chain of dipolarly coupled spin is an highly symmetric system; if the only control available is an external radio-frequency field that acts collectively on all the spins, this symmetry cannot be broken and therefore only a small subspace of the total Hilbert space can be reached by the system during its evolution. If the spin chain is instead of finite length, the symmetry is naturally broken by the boundary conditions. The spins at the extremities of the chain only have one nearest neighbor to which they are strongly coupled. This implies a slightly different energy and also a different dynamics under the internal dipolar hamiltonian with respect to the other spins. This evolution and the control Hamiltonians are still not enough for universal control, as it can be verified by calculating the rank of the Lie algebra generated by the internal and control Hamiltonian (this can be done numerically for small systems of 4-5 spins). However, it is possible to exploit this broken symmetry to create states, where the polarization is localized to the chain ends, and to then examine how this polarization is transported through the chain under the spin-spin couplings.

Our experimental system is fluoroapatite (FAP). The fluorine spins in FAP form linear chains (nearest-neighbor spacing 3.44 Å) separated by an

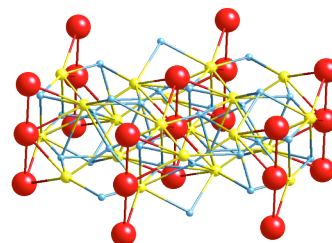


Figure 4

Fluoroapatite

inter-chain distance long enough (9.37Å). The next-nearest neighbor coupling is a factor of 8 times smaller than the nearest neighbor couplings, and the coupling between spins on different chains is about a factor of 30 smaller than the nearest neighbor coupling. If we consider the short-time evolution only, the spin dynamics are dominated by the nearest neighbor interaction. However, at longer times, the longer range interactions lead to a deviation of the spin dynamics from the simple models.

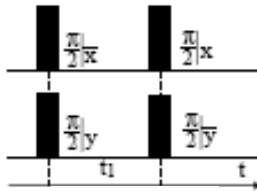


Figure 5

Consider a single chain with a fixed number N of spins, which evolves unitarily under the dipolar hamiltonian and the external control rf field, and decoheres because of its interaction with the environment. The environment therefore includes also the effects of other chains and the distribution in chain composition. In the equilibrium thermal state $\Sigma_i \sigma_z^i$, the polarization is spread equally over the entire spin chain. The pulse sequence shown in Figure 5, combined with phase-cycling, can be used to prepare the initial state $\sigma_z^1 + \sigma_z^N$ from the thermal state. Note that in this

state the polarization is stored only at the ends of the chain.

It is straightforward to understand how the sequence works. Following the first $\pi/2$ -pulse, the dynamics of the end-chain spins is quite different from the dynamics of the internal spins in the chain. When we look at the polarization of individual spins by numerical simulations of 8-10 spin systems (Figure 6), we notice oscillations in polarization of each one of them. In particular the first and last spins have a much slower dynamics (apparent decay) at short time, which is due to the smaller number of couplings.

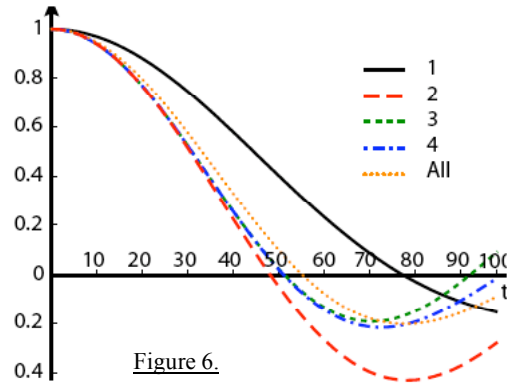


Figure 6.

We can therefore select a time at which the state of the two end spins is still mainly σ_x , while all the other spins have evolved to more complex multi-body states. A second $\pi/2$ pulse will bring the magnetization of spins 1 and N to the longitudinal (z) axis, so that the density matrix describing the system can be written as $\sigma_z^1 + \sigma_z^N + \rho'$. For fluoroapatite we found that the optimal time between $\pi/2$ pulses is 30.3 μ s. Except for very short chains (3-4 spins), the optimal time between pulses is almost independent of the number of spins in the chain, therefore allowing us to choose the time even if we don't know the number of spins in a chain. To select only the desired (first two) terms, we cycle the pulses through different phases, thus averaging to zero all terms which are not either populations or zero quantum terms.

Figure 7 shows the experimentally obtained spectra for an initial thermal state and for the initial state with the polarization only at the chain ends. It is also possible to observe the

signature of these initial states in the multiple quantum dynamics of the spin chain, as the system evolves under the double-quantum (DQ) Hamiltonian. The DQ Hamiltonian is exactly solvable for a 1D system with nearest neighbor couplings, so the experimental results can readily be compared to theory. Figure 8 shows the experimentally measured intensities of the zero and double quantum coherences for the collective thermal initial state (left) and the end-chain selective states (right), as well as the theoretically expected results for a spin chain of 11 spins (assuming nearest neighbor couplings). The agreement is seen to be excellent, indicating that we have indeed created a state with polarization only at the ends of the chain.

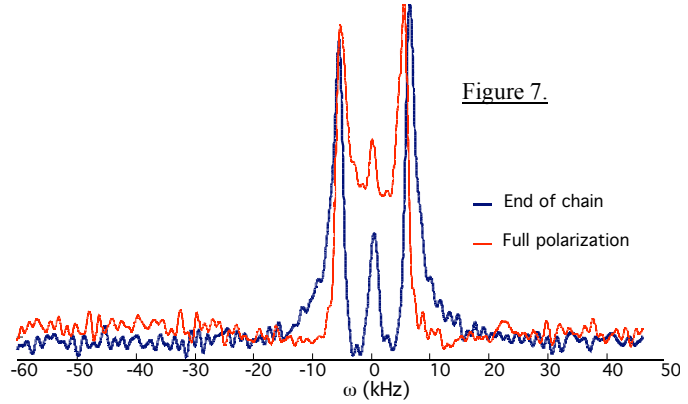


Figure 7.

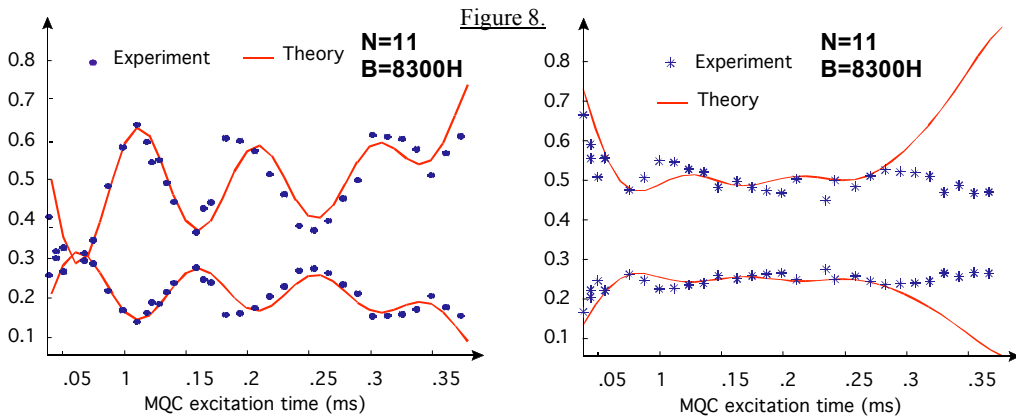


Figure 8.

Polarization transfer driven by the XY and DQ Hamiltonians yield the same result if the number of spins in the chain is odd, while the double quantum Hamiltonian can transfer negative polarization (since it does not conserve the total polarization along the z direction). If we take the absolute value of the polarization, the two Hamiltonians produce the same transport of polarization and therefore the double-quantum Hamiltonian can be used to simulate the flip-flop Hamiltonian that is not available in the system. Figure 9 shows the results of simulations for the transport of polarization under the XY Hamiltonian for an initial state where the polarization is only stored

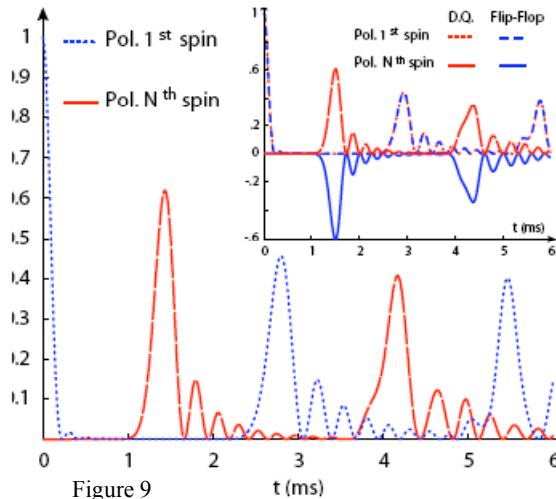
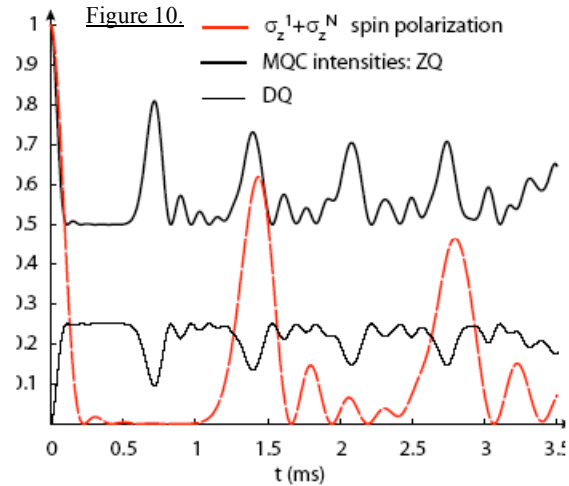


Figure 9

on one end of the spin chain (note we cannot create this state experimentally as yet). The inset shows the transport under the XY and DQ Hamiltonians, showing the similarity between the two.

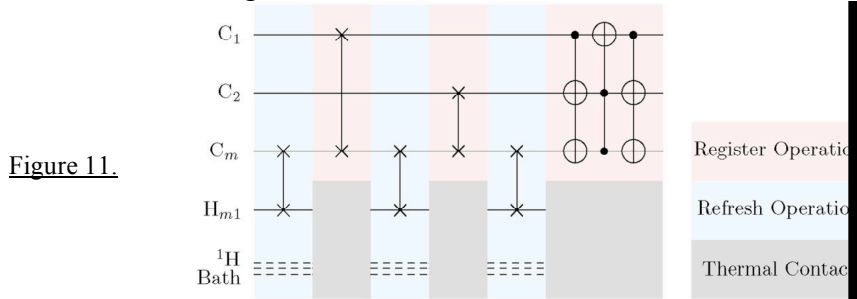
The transport of polarization cannot be detected directly (unless one introduces very strong magnetic field gradients, able to produce an appreciable change of frequency over distances of a few nanometers). It is however possible to monitor the MQC intensities to detect the transfer of polarization. If one is therefore interested in the transfer of polarization from one end of the chain to the other it is possible to follow this transfer driven by the DQ Hamiltonian by measuring the multiple-quantum intensities. In Figure 10 we show how this transport and detection method



would look like for our experimentally prepared initial state with polarization on both ends of the chain. Next-nearest neighbor couplings and cross-chain couplings offer additional pathways that can result in an acceleration of information transport, which has no classical counterpart. This transition from a behavior that can be simulated classically to the more complex quantum behavior is of tantamount importance in the context of QIP, where the efficiency of a quantum computation is obtained by the coherence and interference properties of quantum mechanics.

Control of solid state nuclear spin qubits

We have extended the control techniques developed in liquid state NMR quantum information processing to the control of a three-qubit solid state NMR quantum information processor. The three carbons form the qubits of the system, while the protons are used as the thermal bath. The crystal we use contains 5% ^{13}C enriched malonic acid in a natural abundance lattice. We applied strongly modulating pulses on the malonic acid system to implement an algorithmic cooling protocol in this solid state nuclear spin system shown in the figure below.



The final state correlation fidelity achieved was about 96%. The strongly modulating pulses and the corresponding unitaries are shown in the figure below, along with the spectra obtained.

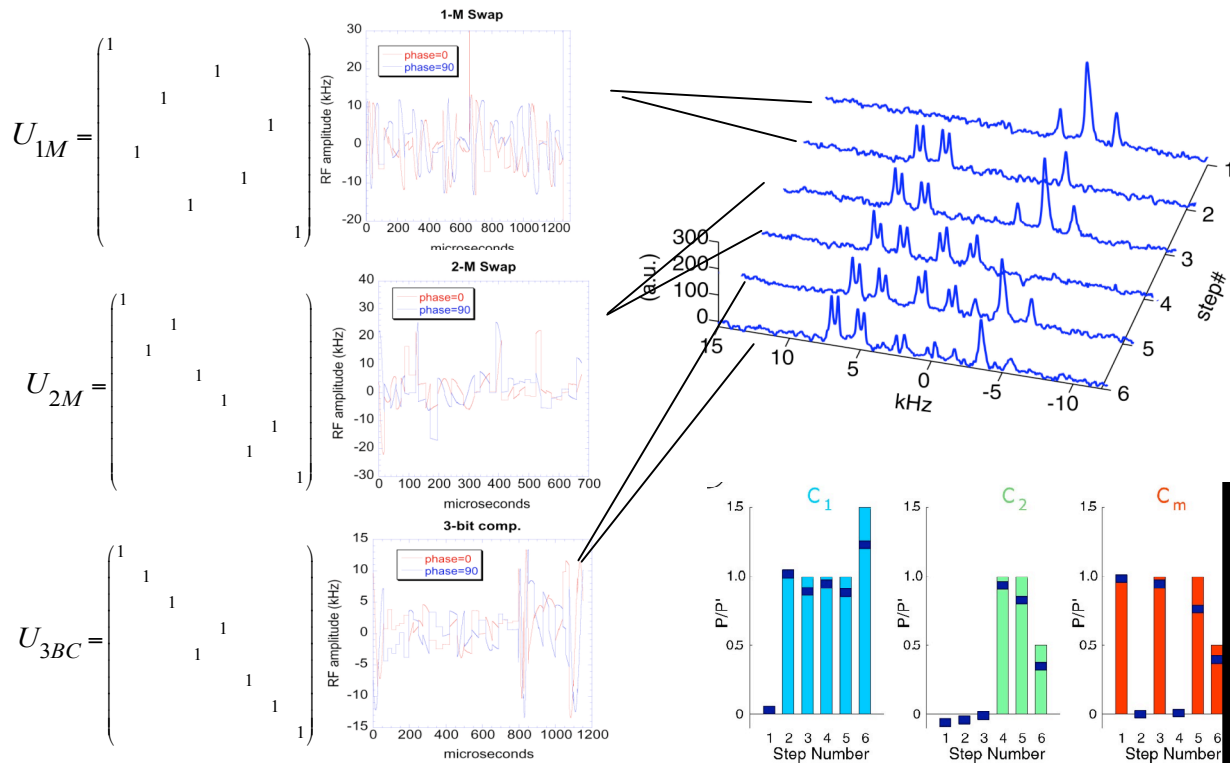


Figure 12. Algorithmic cooling protocol implemented on the 3 qubit solid state NMR system

Electron-nuclear hyperfine couplings

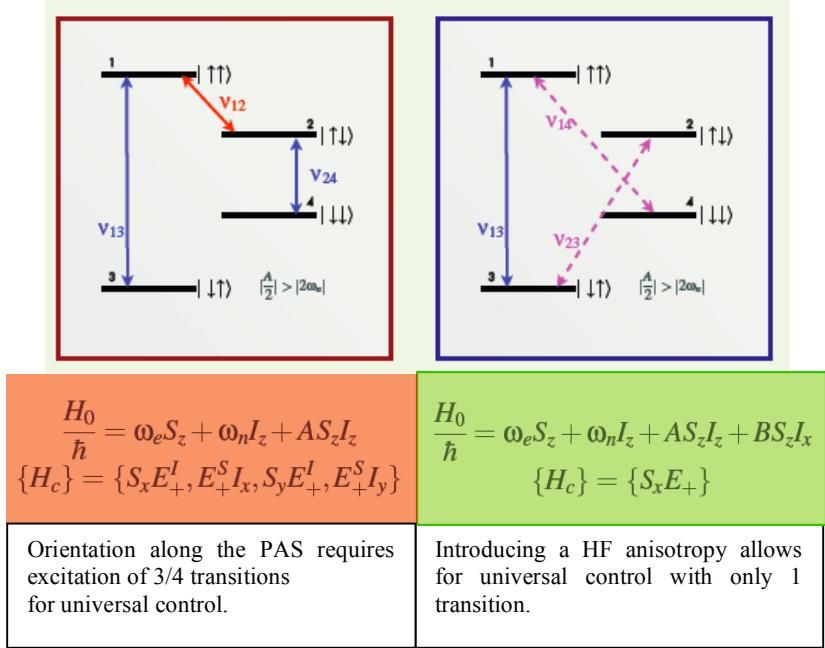
We have proposed a new approach to solid-state quantum computing, the key feature of which is to use an electron/nuclear spin system and to take the best from each. Nuclear spins make great qubits since they have long coherence times, but they are difficult to prepare and readout. Furthermore nuclear/nuclear spin interactions are typically slow, being generally a few kHz. Electron spins have the advantages that they can be prepared in well-defined computational states and individual electron spin readout has been demonstrated. However, electron spins have relatively short coherence times making them difficult to employ for qubits. Fortunately the electron/nuclear spin interaction, the hyperfine coupling, can be quite large, up to a few 100 MHz, and this provides a means for rapid information exchange between electron and nuclear spin systems. So the proposal employs electron spins for state preparation and readout, but the qubits are nuclear spins. The novel element and what makes this approach viable is the mediation of nuclear/nuclear spin gates via the *anisotropic* hyperfine interaction. We have devised a scheme for controlling many nuclear spin states local to a single electron spin where the overall hyperfine coupling of each nuclear spin has an anisotropic form. In such a system, any unitary operation over the nuclear spin system can be created by modulating transitions between the electron spin eigenstates.

Consider an coupled electron-nuclear spin system. In an external magnetic field about a few hundred Gauss, the electron spins are strongly quantized along this external field. The quantization axis of the nuclear spins depends on the relative magnitudes of the nuclear Zeeman energy and the hyperfine coupling strength. At low magnetic fields, the nuclear spins are quantized along the local hyperfine fields, while at high fields the nuclei are quantized along the external field. For moderate field strengths, the nuclear Zeeman energy is comparable to the hyperfine coupling strength and the effective quantization axis lies between the two cases discussed above. Note that in general the hyperfine interaction is a tensorial coupling. If the external field B_0 is along a canonical axis of the hyperfine interaction, the eigenfunctions are product states of $|e,n\rangle$. The transition frequency for an electron spin, is just $\nu_s \pm A/2$. The transition frequency for the nuclear spin is just $\nu_I \pm A/2$. If B_0 is not along a canonical axis of the hyperfine interaction, the eigenfunctions are mixed in the nuclear manifolds. The electron frequencies and nuclear frequencies are geometric means of A, B and ν_I , and forbidden transitions of two spin flips now become allowed. These two situations are compared in Figure 13.

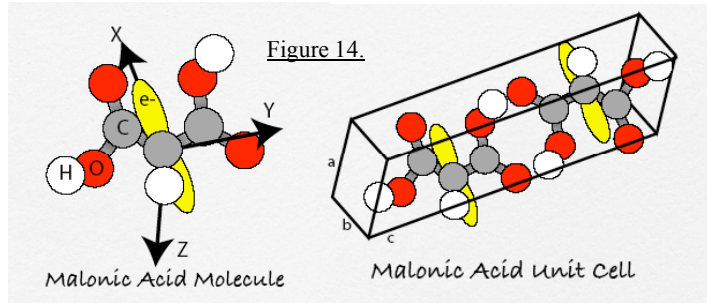
We can examine the controllability of the coupled system in the two cases. Given a system Hamiltonian, H_0 , and independently controllable Hamiltonians $\{H_c\}$, a system is universal if the Lie-algebra generated by the Hamiltonians spans $SU(2^{n+1})$, where one electron spin coupled to n -nuclear spins. Figure 13 also shows the control Hamiltonians that permit universal control in these two systems. While we need to address three of four transitions if the hyperfine coupling has the form $I_z S_z$, we only need to address a single transition if the coupling has the form $S_z \otimes (A I_z + B I_x)$. We can therefore control the nuclear spin system via the electron spins.

In a magnetic field of 0.4 T, the electron and nuclear spin Larmor frequencies are $\omega_s = 11.2$ GHz, and $\omega_l = 17$ MHz (protons). The typical strength of the hyperfine interaction can range from about 2-100 MHz. The typical RF field strengths achievable to rotate the nuclear spins is 200 kHz while the RF field strengths for the electron spins is in the 10 MHz range. The need to apply pulses of the form $E_+^S I_y$ directly to the nuclear spins for the isotropic case on the left of Figure 13, significantly slows down the overall gate speed. The scheme utilizing the anisotropic interaction does not require the application of nuclear spin pulses, and is significantly faster.

Figure 13



Consider the malonic acid system (Figure 14) that has previously been used to show entanglement between an electron and a nuclear spins. Malonic acid is a three-carbon backbone organic molecule that can be grown into a single crystal via evaporative methods. Irradiation of the crystal with 75 keV x-rays produces a unpaired electrons which is highly localized on the middle carbon. The Zeeman splitting of the electron ($S=1/2$) spin is split due to an anisotropic hyperfine interaction with the neighboring proton ($I=1/2$). At low defect densities, the electron-electron dipole interaction can be neglected; the system is thus an ensemble of isolated two-qubit systems. The hyperfine tensor in the principal axis system is (30, 60, 90) MHz. Using techniques originally designed for liquid state NMR, such as strongly modulating pulses and the GRAPE (gradient ascent pulse engineering) algorithm, we can design control schemes for this system.



In our experiments the orientation of the crystal in the external field resulted in ESR frequencies of 12.01 GHz and 11.96 GHz and ENDOR frequencies of 8 MHz and 40 MHz. Figure 15 shows the experimental echo obtained using a GRAPE pulse to perform the $\pi/2$ S_x rotations in a spin echo experiment, in excellent agreement with numerical simulations of the expected echo.

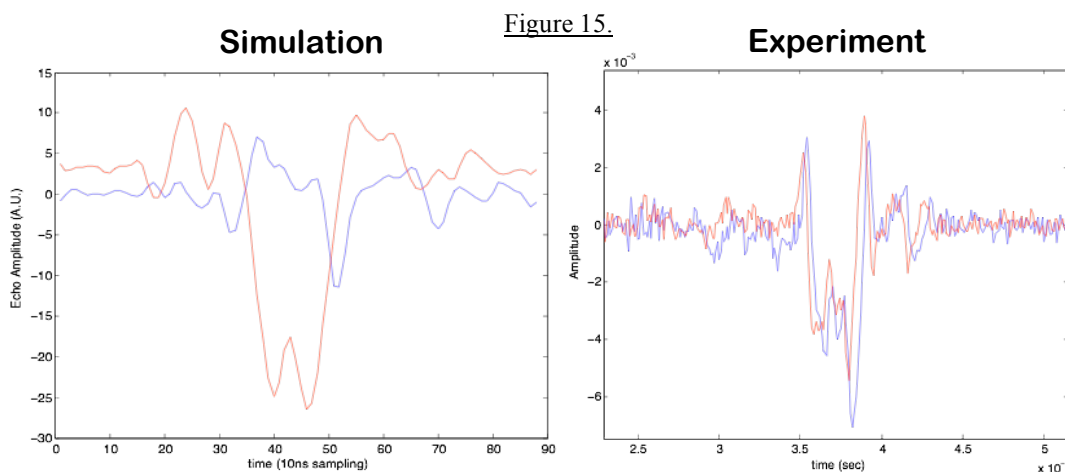


Figure 16 shows the result of the two pulse ESEEM (electron spin echo envelope modulation sequence), using GRAPE pulses. The pulse is also shown in the figure. The frequencies observed are the two ENDOR frequencies as well as the sum (48 MHz) frequency. The expected difference frequency (32 MHz) is not seen very clearly. One of the challenges of the malonic acid system is the bath of dipolar-coupled protons.

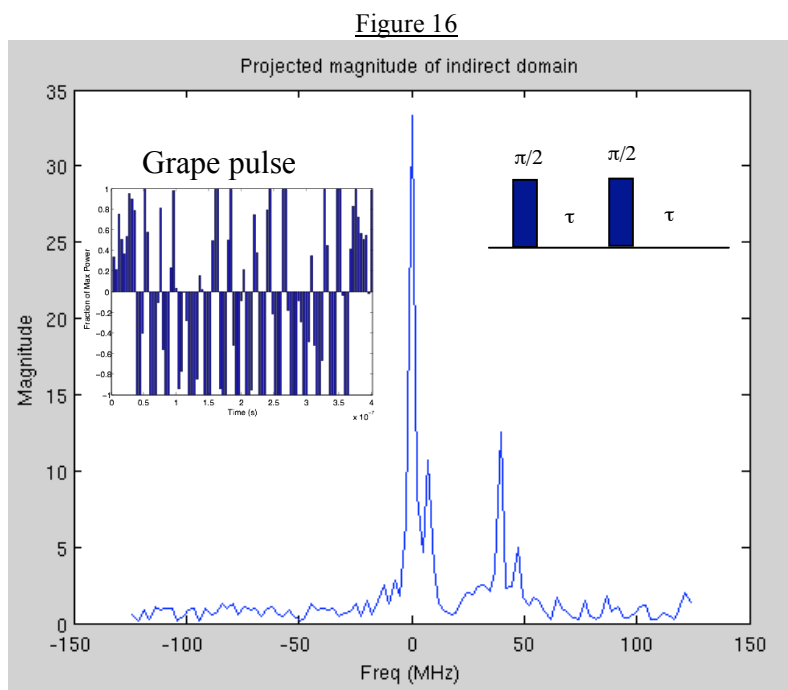
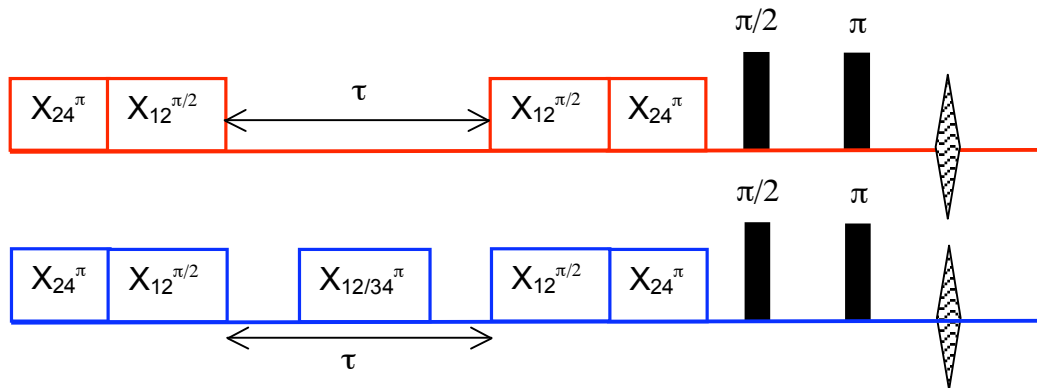
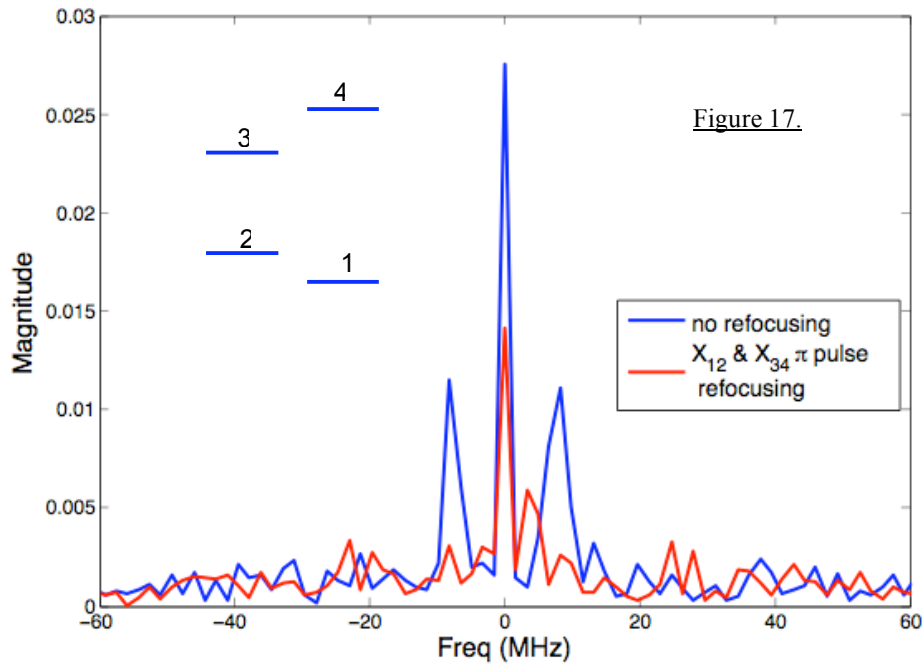


Figure 17 shows the result of two experiments illustrating our ability to control the nuclear spins, using this scheme. In the first experiment (red) we apply a π pulse to the 2-4 transition to create a large population difference on the 1-2 ENDOR transition. We then excite a coherence using a $\pi/2$ pulse on this transition. After a time τ , we transfer the coherence back to a population using another $\pi/2$ pulse, and then transfer this signal

back to the 1-4 transition using a π pulse on the 2-4 transition. Following a short delay, we use a spin echo sequence with hard pulses to measure the signal. The second experiment (blue) is identical to the first except that a refocusing π pulse is applied simultaneously to the 1-2 and 3-4 transitions in the middle of the τ interval. The 1-2 nuclear spin coherence, which evolves at 8 MHz, is not observed in the absence of refocusing, but is clearly seen with the π pulses. The sequences are shown below.

Projected magnitude of FFT wrt τ

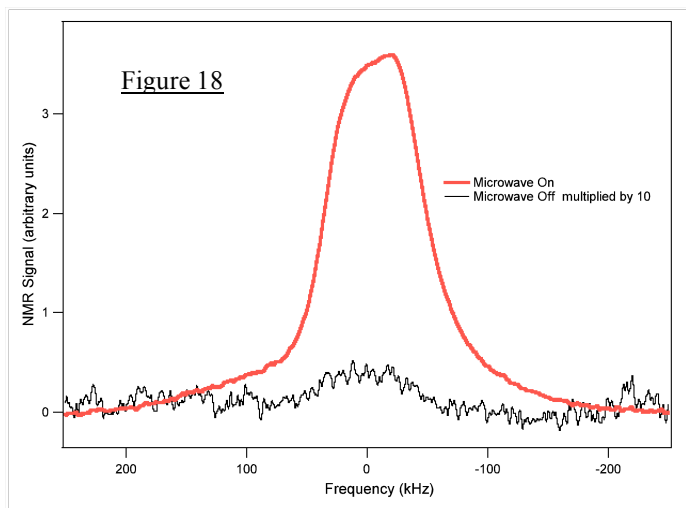


In the presence of multiple nuclear spins it is possible to find subspaces of the nuclear spin system that are protected against electron spin flips. This would allow us to achieve coherence times in the nuclear spin system that are longer than the electron spin T_1 .

Dynamic Nuclear Polarization (DNP)

At room temperature, the nuclear spins are infinitesimally polarized ($\sim 10^{-5}$) in laboratory magnetic fields, and the spin system is highly mixed. As the Zeeman energies are very small the spins remain highly mixed even at liquid helium temperatures. It is necessary to cool the sample to milliKelvin temperatures in order to achieve significant polarization. Alternatively, the spin system can be highly polarized by techniques such as dynamic nuclear polarization which involves polarization transfer from electronic spins, mediated by the hyperfine interaction. The increased polarization will allow us to explore systems with a larger number of qubits, and also allows preparation of the system close to a pure state.

Our DNP setup operates at a field of 2.35T, which corresponds to an electron Larmor frequency around 66 GHz for $g=2$. The system uses a Bruker Avance NMR spectrometer with a home-built probe. Figure 18 shows the NMR spectra of the water-glycerine sample, illustrating a ^1H signal enhancement of 70 produced by dynamic nuclear polarization (DNP) at 1.40 K. The sample consisted of 40 mM of nitroxide TEMPO dissolved in a 40:60 water:glycerol mixture. The top spectrum was obtained after irradiating the sample with microwaves at 65.9 GHz for 53 minutes. The estimated nuclear spin polarization in this experiment was about 12%. The bottom spectrum was obtained under the same conditions but without microwave irradiation. The frequency shift is relative to 100.13 MHz. The enhancement over the room temperature polarization is about 15000. The polarization of the $g=2$ electron spins is 81 % under these conditions. The microwave source used was a 60 mW Gunn diode source (Millitech).

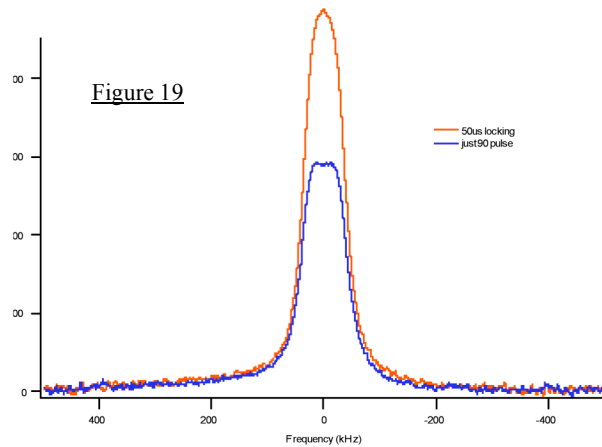


DNP and dipolar diffusion

In the DNP process the initial enhancement is local to the site of the paramagnetic impurity (the electron spin). In order to polarize a bulk nuclear spin system, this process needs to be repeated many times, and the non-equilibrium polarization transported away from the site of the impurity to the bulk. This process is mediated by spin diffusion and is essentially the inverse of the standard T_1 relaxation mechanism in dielectric solids. Spin diffusion is the process by which polarization is transported through a lattice of spins, mediated in most cases by the XY or flip-flop terms of the dipolar interaction. In a high magnetic field, the Zeeman energy and the dipolar energy of the spins are both independently conserved, and have different diffusion and spin-lattice relaxation rates.

In the traditional model, the spins in an inner core around the impurity are essentially frozen in place. They experience a significant local field due to the impurity, and as a consequence they have significantly different Zeeman energies. This energy difference suppresses the XY interaction, creating the so-called "spin-diffusion barrier" around the impurity. In order to transfer polarization across the barrier, an additional source of energy is needed to make up the energy difference between the spins. The nuclear spin dipolar reservoir provides this energy that permits the polarization to cross the barrier. Thus at the site of the impurities the Zeeman and dipolar reservoirs are seen to mix. Once past the spin diffusion barrier, the polarization is transported across the crystal via Zeeman spin diffusion. However, we have recently shown that the diffusion of dipolar order is significantly faster than that of Zeeman order, so the cooling of the dipolar reservoir that is produced locally at the spin diffusion barrier, should quickly be communicated to the bulk. We would therefore expect the effective spin temperature of the bulk dipolar reservoir to be significantly lower than that of the Zeeman reservoir.

Figure 19 shows the signal obtained following a $\pi/2$ pulse, and following a 50 μs spin locking pulse with a weak RF. As this field is comparable to the strength of the local proton dipolar field in the sample, it induces mixing between the Zeeman and dipolar reservoirs. The additional signal enhancement obtained following this mixing indicates that the bulk dipolar reservoir has a lower effective spin temperature than the Zeeman reservoir following microwave irradiation. In fact, given the much smaller heat capacity of the dipolar bath compared to the Zeeman bath at high magnetic fields, the effective temperature of the dipolar system is much colder than that of the Zeeman system. At long times, we would expect the temperatures of the two reservoirs to once again become equal.



We suggest that it is the difference in the spin diffusion rates of the Zeeman and dipolar order that is responsible for the difference in the effective spin temperatures at short times. The faster dipolar diffusion allows a faster cooling of this reservoir. A similar cooling of the dipolar reservoir has also been observed following optical pumping of semiconductor systems such as GaAs and InP. It should be possible to polarize a sample more rapidly by repeatedly cooling the dipolar reservoir and transferring this polarization to the Zeeman reservoir. This transfer of could be done adiabatically using an adiabatic remagnetization in the rotating frame (ARRF). Note that this transfer of order occurs in the bulk crystal, not just locally to the sites of the defects.

Silicon DNP

Patterned ^{29}Si (spin $\frac{1}{2}$) structures on a ^{28}Si (spin 0) substrate are promising for spintronics in general and spin-based quantum computing. Polarizing silicon spins is therefore of significant interest. Here we show the use of DNP to polarize ^{29}Si spins. The electron magnetic moment is about 3500 times larger than the nuclear magnetic moment of ^{29}Si .

We performed DNP experiments on a commercially obtained sample of powdered silicon, and a variety of single crystal samples doped with antimony or phosphorus of varying concentrations. The natural abundance of ^{29}Si in these samples is 4.7 %. Figure 20 shows the DNP enhancement for a sample of Si powder obtained from Alfa Aesar with 99.999% purity, 1-5 μm particles. The ESR signal primarily arises from dangling bonds on the surface of the Si particles in this case. The Si polarization obtained was 5%. The experimental setup was identical to that used in the TEMPO experiments above, except that the RF coil was tuned to silicon.

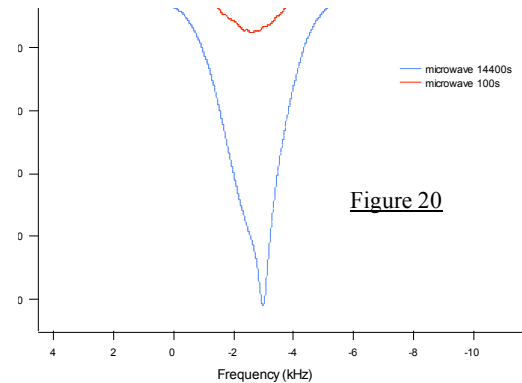


Figure 20

We also performed DNP experiments on antimony (Sb) and phosphorus (P) doped single crystals of silicon. Figure 21 shows the NMR signal from a single crystal of Si doped with Sb at a concentration of $3 \times 10^{17} \text{ cm}^{-3}$. Figure 22 shows the growth of the DNP enhanced signal as a function of the microwave irradiation time, and as a function of microwave power. We used a 100 mW Gunn source, and a 1 W custom-built source from Quinstar Technologies. The 1 W source consists of 2 Impatt diode sources, both injection locked with a Gunn in order to reduce the phase noise, whose outputs are combined. The data seems to indicate that the B_1 field at the site of the spins is still too low to efficiently drive the DNP process.

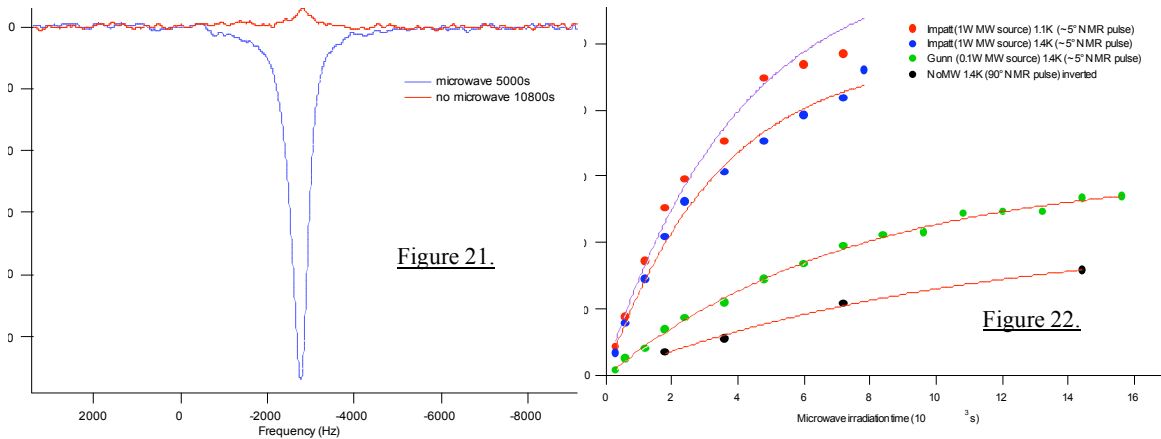


Figure 21.

Figure 22.

We replaced the horn antenna with a cylindrical TE₀₁₁ resonator in order to increase the cavity Q and hence the B₁ field produced, and performed DNP experiments on a new sample of P-doped Si wafers with a doping concentration of $2 \times 10^{17} \text{ cm}^{-3}$. We also setup a Roots blower to pump the helium space and lower the temperature in our cryostat to 1.1 K. This increases the electron spin polarization to 89%. Figure 23 show the ²⁹Si spectrum from this sample after microwave irradiation of the sample

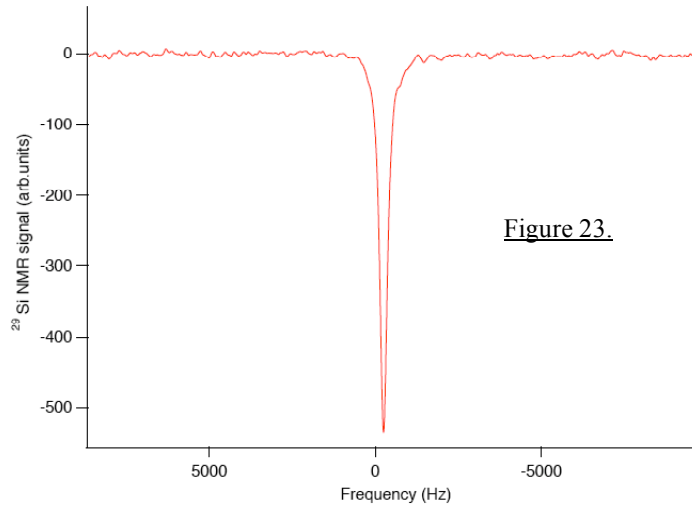


Figure 23.

at 65.86 GHz for 2 hours. During irradiation the sample was placed inside the cylindrical cavity and was subsequently moved to rf coil outside of the cavity for detection. The maximum DNP enhancement obtained was about 200, corresponding to the nuclear spin polarization of 8.3%. The frequency shift is relative to 19.89 MHz.